

Heterogeneous dynamics during deformation of a polymer glass

Robert A. Riggleman^{1,†}, Hau-Nan Lee^{2,†}, M. D. Ediger², and Juan J. de Pablo³

† - *These two authors contributed equally to this work*

1 Department of Chemical Engineering,

University of California, Santa Barbara, CA 93106

2 Chemistry Department, University of Wisconsin, Madison, WI, 53706

3 Department of Chemical and Biological Engineering,

University of Wisconsin, Madison, WI, 53706

Abstract

The origins of molecular mobility in polymer glasses, particularly under deformation, are not well understood. A concerted experimental and computational approach is adopted to examine the segmental motion of a polymeric glass undergoing creep and constant strain rate deformations. Through a combination of molecular dynamics simulations and optical photobleaching experiments we are able to directly probe how dynamic heterogeneity evolves during deformation. Two distinct regimes emerge from our analysis; early in the deformation, the dynamics of the glass are strongly heterogeneous, as evidenced by the spectrum of relaxation times measured experimentally and the participation ratio of the atomic non-affine displacements measured computationally. After the onset of flow, the dynamics become significantly more homogeneous, and the participation ratio increases considerably.

Glasses are arguably one of the most intriguing states of condensed matter. Emerging uses of polymeric glasses in high-performance situations, including aviation and medical applications, require that their response to repeated cycles of stress and strain be understood. Polymer glasses are said to undergo “physical aging” with time [1]; their molecular motion slows down as time passes. It is also generally appreciated that, upon deformation, the dynamics in a polymer glass can accelerate in a process sometimes described as “rejuvenation”. Aging and rejuvenation have traditionally been considered in the context of macroscopic mechanical experiments[2], but the molecular processes responsible for such behaviors have seldom been directly observed. In the absence of detailed molecular-level observations, theoretical descriptions of stress-induced rejuvenation have largely relied on Eyring’s idea that an applied stress lowers the energy barriers that, inhibit molecular motion in a glass[3]. Eyring’s model, however, does not consider a variety of phenomena, including dynamic [4] and mechanical [5, 6] heterogeneity, strain hardening [7, 8], and the dependence of mobility with deformation rate after flow onset[9].

In particular, recent experiments of Lee *et al.* have shown that the segmental mobility of glassy poly(methyl methacrylate) (PMMA) can be enhanced by a factor of 1000 during creep deformations[9]; their observations cannot be explained in terms of Eyring’s theory. Lee *et al.* relied on dilute fluorescent probe molecules and a photobleaching technique for their measurements. If one assumes that probe molecules are faithful reporters of the dynamics of the surrounding polymer matrix, their measurements suggest that molecular mobility is vastly enhanced and becomes more homogeneous after flow onset, and that it is reduced in the strain-hardening regime. It is unknown whether flow influences the probe molecules or the polymer molecules to different extents, and this remains an important consideration. Having an otherwise solid material enter a regime of homogeneous, liquid-like flow through the mere exertion of stress could have far-reaching consequences, including strategies for annealing or prevention of failure. From a scientific point of view, providing a detailed molecular interpretation of Lee *et al.*’s deformation-induced transition from an elastic material (with little molecular mobility) to a homogeneous and mobile material would provide a much needed mechanistic explanation that would impact not only our understanding of polymer glasses, but also that of “jammed” systems [10].

Experimental studies of the influence of deformation on the dynamics of glassy polymers have been limited. Recent simulations, however, have examined the deformation of small-

molecule glasses [11–13] and polymer glasses [14–18]. In both classes of materials, results of simulations have revealed that molecular mobility is enhanced with deformation, often by many orders of magnitude depending on the deformation rate [11, 18]. Simulations have also suggested that, consistent with Eyring’s proposition, deformation leads to a reduction of the energy barriers that impede relaxation [13], and that the material’s position on its potential energy landscape is coupled to its dynamics [17].

It is generally appreciated that glasses exhibit dynamical heterogeneities, and that such heterogeneities disappear as the material is heated far above T_g . One of the central questions addressed here is whether deformation has the same effect as temperature. We measure the rotational dynamics of fluorescent probe molecules dispersed in a PMMA glass through photobleaching experiments and examine molecular events during deformation through molecular dynamics simulations. A direct comparison of experimental observations and computational results serves to address two issues. First, it helps establish that probe molecules act as inert reporters of polymer segmental dynamics. Second, it demonstrates the validity of our model and the results from high deformation rate simulations, adding credence to our subsequent molecular interpretation of experimental observations. Our concerted experimental and computational approach reveals that at least two distinct deformation regimes exist. In the first of these, deformation-induced molecular mobility is highly heterogeneous, consisting of collections or clusters of molecules that move much faster than the majority of the sample. A flow regime is then entered, segmental mobility is considerably faster than at rest, and the dynamics become homogeneous. Upon removal of the stress, the material gradually recovers its glassy nature and returns to a dynamically heterogeneous state.

Our experiments were conducted on PMMA glass samples at $T = 375.7K$. Trace amounts of a fluorescent probe molecule (DPPC, N,N’-Dipentyl-3,4,9,10-perylenedicarboximide) were used to measure relaxation under constant tensile, uniaxial, engineering stress (σ_E). During a creep deformation, 37 photobleaching experiments were performed to monitor the mobility of the probe molecules; these probes are perceived to be good reporters of the segmental dynamics of PMMA [19]. More specifically, the photobleaching experiments measure the anisotropy decay function, $r(t)$, which describes the rotational dynamics of the probe molecule. The mobility changes were quantified by first fitting that function to a KWW stretched exponential, $r(t) = r(0) \cdot e^{-(t/\tau)^\beta}$, where β is the so-called stretching exponent and measures the breadth of the distribution of relaxation times present in the system. The

rotational correlation time, τ_C , was obtained by integrating the KWW function. The mobility shift factor was defined as $a = \tau_C/\tau_{C,0}$, where the 0 subscript denotes an estimate of τ_C at rest (without deformation). In the absence of an applied stress, the values of τ_C and β for our PMMA samples were found to be approximately 51000s and 0.32, respectively. Complete experimental details can be found elsewhere [9].

Our simulations are carried out on an entangled coarse-grained polymer model in which polymer molecules consist of 500 Lennard-Jones (LJ) interaction sites connected by stiff harmonic bonds. The non-bonded interactions are described by the LJ potential, and both LJ parameters σ and ϵ are taken as unity. All simulation results are reported in LJ reduced units and denoted by a *. Additional details about our model can be found in the literature [17, 18, 20]. A combination of double rebridging Monte Carlo (MC) techniques [21, 22] and molecular dynamics was used to generate independent equilibrium configurations of the polymer at $T^* = 1.2$ and $P^* = 0.3$. After equilibration, we cooled three independent configurations to $T^* = 0.35$ at a rate of $\Delta T^*/\delta t^* = 10^{-4}$; at this cooling rate, T_g^* for our polymer is 0.370 ± 0.001 , as determined from identifying the discontinuity in plots of density vs. temperature. All results are averages over each configuration; the reported uncertainties correspond to the standard error for the values obtained from each configuration. Each sample was aged at $T^* = 0.35$ for $t^* = 10000$ prior to deformation. Similar to the experiments, we performed creep deformations by applying a tensile true stress in the x -direction while maintaining $P^* = 0.30$ in the y - and z -directions.

The dynamics during deformation simulations were quantified in terms of the bond autocorrelation function $C_b(t)$, which measures the rotational mobility of the bonds along the polymer backbone. Effective relaxation times (τ_b) from the simulations were extracted from $C_b(t)$ by fitting to the KWW stretched exponential function and integrating, as described above for the experiments. The value of τ_b prior to deformation was estimated from a long MD simulation at $T^* = 0.35$ to be $\tau_{b,0} = 180000 \pm 60000$; $C_b(t)$ was calculated repeatedly during our deformations using time windows [17, 18] of size $t^* = 1000$.

Fig. 1a shows the (true) strain response to a multi-step creep experiment. Immediately after applying the stress, the strain goes through a fast elastic deformation, followed by a prolonged period of slow deformation where the strain rate decreases. Approximately 7500s after applying the stress, the strain rate goes through a minimum and the material begins to flow until the stress is reduced at 11000s; this minimum in the strain rate is the onset

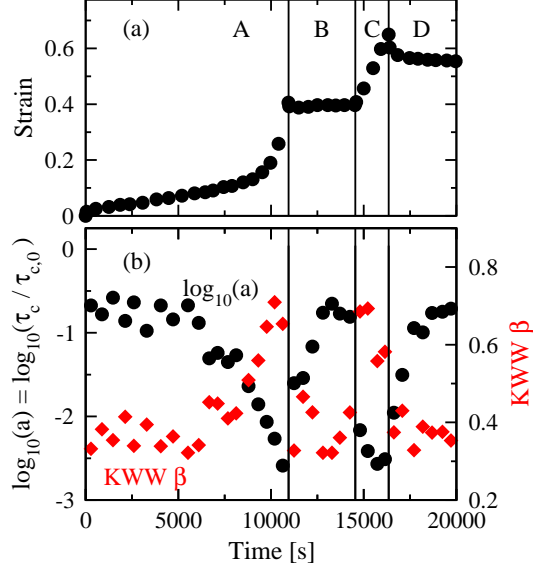


FIG. 1: (color online) (a) Experimental results for the strain as a function of time for the multistep creep deformations. The vertical bars indicate the time at which σ_E was changed, and the applied stresses were 14.9, 5.75, 14.9, and 0.43MPa in periods A, B, C, and D, respectively. (b) Mobility (\circ) and the KWW exponent β (\diamond) as a function of time during the multistep creep experiment.

of flow. Fig. 1b plots the changes in the mobility and the KWW β parameter during the multistep creep deformations. Immediately after the stress is applied, the mobility jumps by nearly one order of magnitude and increases gradually until the onset of flow, where it changes rapidly as the strain rate increases. β does not exhibit any significant changes until the onset of flow, where β begins to increase, reaching a maximum of 0.75 before the stress is reduced.

When the stress is reduced at 11000s, both the mobility and β immediately decrease; β fluctuates around 0.40 and the mobility continues to decrease until the stress is again increased at 14500s. Although the mobility is reduced compared to the first step of the creep experiment, at no point does it return to the undeformed value. After the stress is increased at 14500s and subsequently removed during the final two steps of the multistep creep experiment, we find that the above trends repeat themselves: when the stress is high and the material is flowing (strain rate increasing), the mobility increases, and the changes in β indicate that the dynamics become more homogeneous. When the stress is removed, the mobility decreases and β decreases towards its value at rest.

Fig. 2a shows the strain response during the multi-step creep simulation. All of the mechanical features of the experiments are reproduced in the simulations: early in the deformation there is a rapid elastic response followed by a brief period where the strain rate decreases ($t^* < 300$). Beyond this point, the strain rate increases as the material begins to flow until the stress is reduced at $t^* = 2000$. Fig. 2b plots the simulated changes in mobility; similar to the experiments, there is a rapid decrease in τ_b by approximately one order of magnitude upon the application of stress. The mobility continues to increase until $t^* = 2000$, where the stress is reduced from 0.62 to 0.20. The strain response exhibits a fast elastic retraction followed by continued elongation at a low strain rate. The mobility decreases by approximately one order of magnitude but remains nearly an order of magnitude faster than that in the undeformed sample. In the final two steps of the multi-step creep simulation, where the stress is again increased at $t^* = 6000$ and removed entirely at $t^* = 10000$, these trends repeat themselves. Under large stress, the material deforms at a high strain rate and the mobility becomes much faster, while the polymer glass slowly recovers and the mobility decreases sharply when the stress is removed. Together, Figs. 1 and 2 show that the simulations capture all of the major features of the strain response and mobility observed in multi-step creep experiments, a finding made even more remarkable knowing that the simulations and experiments are sampling very different time scales.

The KWW exponent β and its changes with deformation are particularly relevant to any discussion of dynamic heterogeneity. For the undeformed polymer model $\beta = 0.76 \pm 0.05$, and we expect β to cover a range between its undeformed value and unity. Unfortunately, given the uncertainty on β and the limited range we expect β to cover, it is difficult to discern a clear dependence of β on deformation. We therefore characterize the dynamic heterogeneity in our simulations by characterizing the non-affine molecular displacements. If all polymer segments moved solely as a result of an imposed macroscopic strain they would move affinely. In an amorphous polymer glass they rarely do so [23], and the non-affine displacements simply measure the deviations of all particles in the system from their affine positions [20, 23, 24]. The non-affine displacement vector for particle i is denoted by $\mathbf{r}_{i,\mathbf{NA}}$, and a participation ratio (P_R) for the non-affine displacements is defined by $P_R = \langle r_{NA}^2 \rangle^2 / \langle r_{NA}^4 \rangle$, where the angular brackets indicate an average over all particles. P_R characterizes the fraction of particles involved in non-affine motions and ranges from 1.0 (when all of the particles have the same $|\mathbf{r}_i^{\mathbf{NA}}|$ and motion is homogeneous) to $1/N$ (when only one particle has a finite

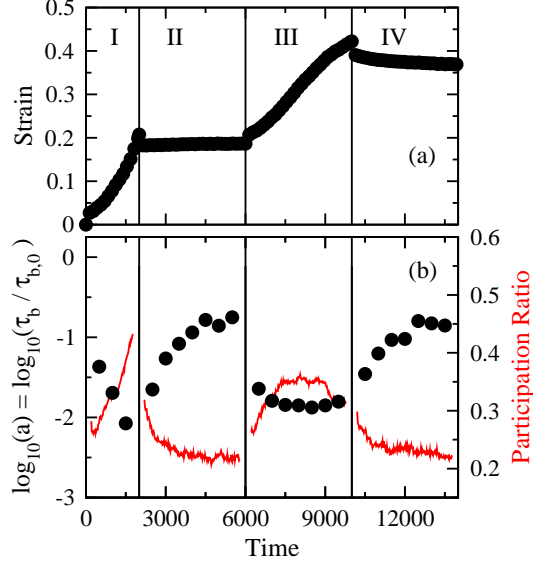


FIG. 2: (color online) (a) Simulation results for the strain as a function of time for the multistep creep deformations. The vertical bars indicate the times where σ_T^* was changed, and the applied stress were 0.62, 0.20, 0.62, and 0.0 in periods *I*, *II*, *III*, and *IV*, respectively. (b) Mobility (points) and participation ratio (line) as a function of time during the multistep creep deformations.

$|\mathbf{r}_i^{\text{NA}}|$ and motion is heterogeneous). Fig. 2b shows P_R as the multi-step creep deformation proceeds. The non-affine displacements used to calculate P_R are determined relative to configurations separated by $t^* = 400$. For example, P_R calculated at $t^* = 1000$ is taken relative to the configuration at $t^* = 600$; the time that we associate with this point is taken as the midpoint, $t^* = 800$. In the first step of the creep deformations P_R monotonically increases, implying that a larger fraction of the system is participating in the molecular motion of the material, and the dynamics become homogeneous with flow. This increase of P_R is consistent with the increase in β observed in the experiments in Fig. 1b at the onset of flow. For the remaining three steps of the multi-step creep deformation, P_R continues to mirror the trends observed in the KWW β depicted in Fig. 1b. In the two steps where the stress is low or zero (steps *II* and *IV* in Fig. 2a), P_R decreases, implying more heterogeneous dynamics while P_R increases rapidly in the steps where the stress is high (steps *I* and *III*).

The increase in P_R after the onset of flow is particularly intriguing, and provides an indication in the simulations that the nature of the dynamics change qualitatively at the onset of flow. It is instructive to affirm the connection between the minimum in the participation

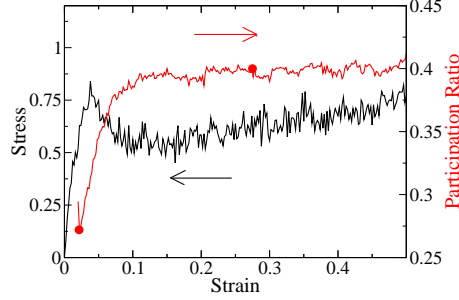


FIG. 3: (color online) Stress (black line, left y -axis) and participation ratio (red line, right y -axis) as a function of strain for a constant true strain rate deformation at $\dot{\gamma} = 10^{-4}$. The circles indicate the configurations shown in Fig. 4 below.

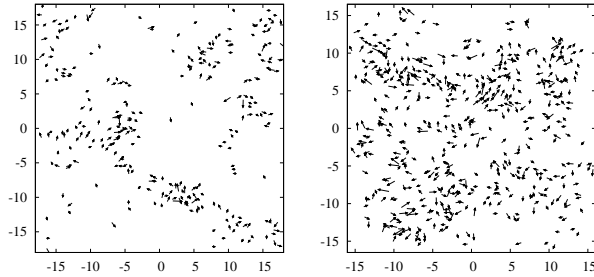


FIG. 4: Two-dimensional projection of the nonaffine displacements at the two points indicated in Fig. 3: near the minimum (a) and the maximum of P_R (b). The projection is in the plane perpendicular to the axis of deformation; displacements greater than 30% of the maximum nonaffine displacement are shown.

ratio and the onset of flow by deforming the simulated glasses at constant strain rate, where the yield point also corresponds to the onset of flow. In Fig. 3, we plot the stress-strain curve and the evolution of P_R resulting from a constant strain rate deformation at a tensile strain rate of $\dot{\gamma} = 10^{-4}$. At the yield point, P_R begins at a minimum value of approximately 0.28 and increases towards 0.40, which is on the order of the maximum value observed in the multi-step creep deformations above.

We can complete the picture of how dynamic heterogeneity arises and changes in a polymer glass during deformation by simply examining images of the displacement fields at the minimum and near the maximum of P_R . In Fig. 4 we have chosen an arbitrary x cross section and plotted the projection of the non-affine displacement vectors in the y - z plane at

the two points indicated in the P_R curve in Fig. 3. There is a stark contrast between these two images; at the onset of flow, where P_R is relatively small and the experimental β is still close to its undeformed value, the dynamics are strongly heterogeneous, and the areas of high mobility are relatively small in size. However, beyond the onset of flow, the simulated P_R and the experimental β both increase. Fig. 4b demonstrates that the dynamics become significantly more homogeneous, and the effect of deformation on dynamic heterogeneity is more significant than temperature. When the mobility changes by a factor of 800 in the experiments presented here, β increased from 0.32 to 0.75. When the temperature is increased to achieve a similar change in the mobility, β remains unchanged [9].

Our results help establish that the dynamics of probe molecules in a polymer matrix under active deformation are faithful reporters of molecular mobility in a polymer glass. Our simulations provide a direct interpretation of our experiments in which, at small deformations, molecular rearrangements are localized and occur through clusters of molecules moving in unison. As the deformation proceeds through the onset of flow, mobility increases dramatically, and the motion becomes more homogeneous. At large deformations one enters a strain hardening regime in which molecular mobility is again decreased. We anticipate that the molecular-level experimental observations and their mechanistic interpretation provided here will lead to improved theories for the non-linear deformation behavior of polymeric materials and jammed systems.

-
- [1] L. C. E. Struik, *Physical Aging in Amorphous Polymers and Other Materials* (Elsevier, New York, NY, 1978).
 - [2] H. E. H. Meijer and L. E. Govaert, *Prog. Polym. Sci.* **30**, 915 (2005).
 - [3] H. Eyring, *J. Chem. Phys.* **4**, 283 (1936).
 - [4] M. T. Cicerone and M. D. Ediger, *J. Chem. Phys.* **104**, 7210 (1996).
 - [5] K. Yoshimoto, *et al.*, *Phys. Rev. Lett.* **93**, 175501 (2004).
 - [6] F. Léonforte, *et al.*, *Phys. Rev. Lett.* **97**, 055501 (2006).
 - [7] R. S. Hoy and M. O. Robbins, *J. Polym. Poly. B: Polym. Phys.* **44**, 3487 (2006); *Phys. Rev. Lett.* **99**, 117801 (2007).
 - [8] H. G. H. van Melick, L. E. Govaert, and H. E. H. Meijer, *Polymer* **44**, 2493 (2003).

- [9] H.-N. Lee, *et al.*, J. Chem. Phys. **128**, 134902 (2008); Science **323**, 231 (2009).
- [10] P. Schall, D. A. Weitz, and F. Spaepen, Science **318**, 1895 (2007).
- [11] L. Berthier and J.-L. Barrat, J. Chem. Phys. **116**, 6228 (2002).
- [12] M. Nandagopal and M. Utz, J. Chem. Phys. **118**, 8373 (2003).
- [13] D. J. Lacks and M. J. Osborne, Phys. Rev. Lett. **93**, 255501 (2004).
- [14] F. M. Capaldi, M. C. Boyce, and G. C. Rutledge, Phys. Rev. Lett. **89**, 175505 (2002).
- [15] A. V. Lyulin *et al.*, Macromolecules **37**, 8785 (2004).
- [16] M. Warren and J. Rottler, Phys. Rev. E **76**, 031802 (2007).
- [17] R. A. Riggleman, K. S. Schweizer, and J. J. de Pablo, Macromolecules **41**, 4969 (2008).
- [18] R. A. Riggleman *et al.*, Phys. Rev. Lett. **99**, 215501 (2007).
- [19] R. Bergman *et al.*, J. Non Cryst. Solids **235**, 580 (1998).
- [20] H.-N. Lee *et al.*, Macromolecules, submitted (2009).
- [21] N. C. Karayiannis, V. G. Mavrantzas, and D. N. Theodorou, Phys. Rev. Lett. **88**, 105503 (2002).
- [22] B. J. Banaszak and J. J. de Pablo, J. Chem. Phys. **119**, 2456 (2003).
- [23] G. J. Papakonstantopoulos *et al.*, Phys. Rev. E **77**, 041502 (2008).
- [24] F. Léonforte, *et al.*, Phys. Rev. B **72**, 224206 (2005).
- [25] We are grateful for funding from the National Science Foundation (NIRT 0506840) and for useful discussions with Ken Schweizer and Jim Caruthers.